Building footprint layers show that flooding risk increased more due to greater building exposure than to greater peak discharge with urbanisation in SE France

Dennis M Fox, Mostafa Banitalebi, Anne Rainaud

Journal of Hydrology: Regional Studies 54 (2024) 101882

Contents lists available at ScienceDirect

Journal of Hydrology: Regional Studies

journal homepage: www.elsevier.com/locate/ejrh

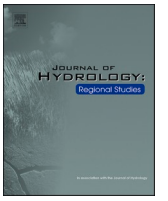

Building footprint layers show that flooding risk increased more due to greater building exposure than to greater peak discharge with urbanisation in SE France

Dennis M. Fox [a,*], Mostafa Banitalebi [a], Anne Rainaud [b]

[a] Université Côte d'Azur, UMR ESPACE CNRS, Nice 06204, France
[b] Université Côte d'Azur, CERDACFF, Nice 06050, France

ARTICLE INFO

Keywords:
Urbanisation
Building footprint
Imperviousness
Flood risk policy
Hydrologic modeling
Hydraulic modeling

ABSTRACT

Study region: South-east Mediterranean France
Study focus: Urbanisation and climate change are producing unprecedented flood risks. Urbanisation increases storm peak discharge and flooded area. Building in the flood plain exposes more people and infrastructure to floods. This study examines the impact of urbanisation over 3 decades (1988/90–2020) on flood risk in SE France. Building footprint layers were used to quantify urban growth, and peak discharge and flooded area were modeled for 3 12-hr rainfall events: 80 mm, 140 mm, and 200 mm. Building growth ranged from 28 % to 65 %. Total imperviousness grew at a rate that was equal to or greater than built area. The relative increase in peak discharge was greatest for the 80-mm event (+12.2 %) and diminished to its lowest value for the 200-mm event (+2.4 %).
New hydrological insights for the region: Flooded area increased proportionately to changes in peak discharge, but mean growth in flooded building footprint area was almost 43 times greater than growth in flooded area. New buildings within the flooded perimeter contributed more to flood risk than changes in peak discharge and flooded area. Planning legislation limited growth close to channels, but flood risk grew rapidly beyond in less restricted areas. Building footprint data provide an accurate approach to mapping changes in flood risk with urbanisation.

1. Introduction

The number of people living in cities will increase from about 55.3 % in 2018 to 68.4 % in 2050; this represents an addition to urban environments of close to 2.5 billion people (Angel et al., 2011; United Nations, 2019). As cities expand, large swaths of agricultural and natural land are converted to urban and suburban uses, and in some cases expansion rates of cities can be as much as twice their demographic growth (Angel et al., 2011). Urban, suburban, and industrial/commercial expansion (called 'urbanisation' or 'urban expansion' from here on) includes the addition of buildings, roads, sidewalks, parking lots, and other impervious surfaces to the landscape. Studies have consistently shown that imperviousness increases storm runoff and peak discharge and shortens lag time (Arnold and Gibbons, 1996; Jacobson, 2011; Sohn et al., 2020; Wagner et al., 2016). Urban expansion and increased imperviousness therefore have a direct impact on runoff dynamics and flood risk for a given storm. In addition to increasing runoff, building in the

* Corresponding author.
E-mail address: dennis.fox@univ-cotedazur.fr (D.M. Fox).

https://doi.org/10.1016/j.ejrh.2024.101882
Received 18 April 2024; Received in revised form 15 June 2024; Accepted 23 June 2024
Available online 17 July 2024

flood plain exposes more people and infrastructure to floods (Nguyen et al., 2021), so imperviousness is both a cause and a victim of floods. López-Martínez et al. (2017) indicate that exposure to flooding increased by more than 250 % along the Spanish Mediterranean coast due to a lack of spatial planning. Similarly, Barredo et al. (2012) attribute the increased cost of flood damage insurance claims between 1971 and 2008 in Spain to a substantial increase in exposure. Land use changes in potential flood zones is recognized as a major factor in flood risk, superior even to climate change (Winter and Karvonen, 2022).

One method of estimating changes in imperviousness is through its direct impact on runoff (Alley and Veenhuis, 1983; Boyd et al., 1993; Ebrahimian et al., 2016), but remote sensing and Geographic Information Systems (GIS) techniques have become the most frequently-used approach for measuring total impervious area (Jacobson, 2011). These estimations, however, are not faultless as concrete or asphalt and bedrock or bare soils can be confused. In addition, shade effects from buildings and tree canopies in urban environments can mask impervious surfaces or create further confusion between categories (Myeong et al., 2001; Wu and Murray, 2003; Yang and Li, 2015). One way of dealing with this is by combining a GIS vector building footprint layer with very high spatial resolution (≤50 cm) aerial photographs to quantify imperviousness (Fox et al., 2019).

The combination of urbanisation and climate change contribute to greater peak discharges (Ahiablame et al., 2017) and more frequent large floods in Europe (Kundzewicz et al., 2013) that are expected to increase flood damage in future (Feyen et al., 2012). The frequency of extreme events, and to a lesser degree, the magnitude of these events, is expected to increase for most regions of the world in the coming decades (Papalexiou and Montanari, 2019). The predicted impacts of climate change vary according to the time-step at which rainfall events are analysed, and more particularly on the presence of skewness in the distribution of extreme events, which is greater at shorter (hourly) time-steps than daily values (De Luca et al., 2024). As rainfall distributions evolve with climate change, historical statistics of return periods lose in accuracy (Vautard et al., 2015), and land use planning legislation, defined by historical events or hydraulic modeling of empirical rainfall return periods, is increasingly disconnected from actual flood risk (López-Martínez et al., 2017). Vautard et al. (2015) observed a 30 % increase in daily autumn rainfall maxima in southern France since the middle of the 20th century; this corresponds to a 4 % per decade increase between 1950 and 2014. The authors attribute this trend to increasing fall temperatures that drive greater atmospheric moisture contents as September temperatures are reported to be 1.1°C warmer in 2014 than in 1950; this corresponds to a warming trend that is 50 % faster than global mean temperatures. They also note that the probability of experiencing the most extreme event of the times series (which occurred in 2014) has tripled since 1950. Others have also observed increases in mean rainfall intensity, more frequent events exceeding 200 m day^{-1}, and greater areas affected by high intensity rainfall events between 1961 and 2015 (Ribes et al., 2019).

In France, municipal flood risk planning legislation was first introduced in 1982 for insurance reasons, and it incited municipal councils to integrate risk exposure maps in their planning documents. Official Risk Prevention Planning (PPR) documents became compulsory for all French municipalities starting in 1995, but it took most municipalities years to implement the new rules. A more global approach was introduced in the National Flood Risk Management Strategy (SNGRI) in 2014 which attempts to combine a regional approach with local considerations. These rules take into account both potential runoff storage applications and imperviousness thresholds.

Coastal urbanization in the Mediterranean region continues to progress despite legislation to limit development (Prévost and Robert, 2016; Smiraglia et al., 2023). Building in the alluvial plain presents several advantages: the terrain is flat and usually well-connected to the main road network, and laying electrical lines, communication lines, and drinking and wastewater pipes is cheaper and faster in non-cohesive alluvial soils than in bedrock. The south of France has experienced unprecedented catastrophic flood events in recent decades with dozens of fatalities and billions of euros in damage. The Alpes-Maritimes department alone, located in SE France, has experienced two devastating storms in the past decade with close to 40 cumulated fatalities and hundreds of millions of euros in damage. Like elsewhere, the severity of these events is sometimes attributed to poor urban planning and sometimes to

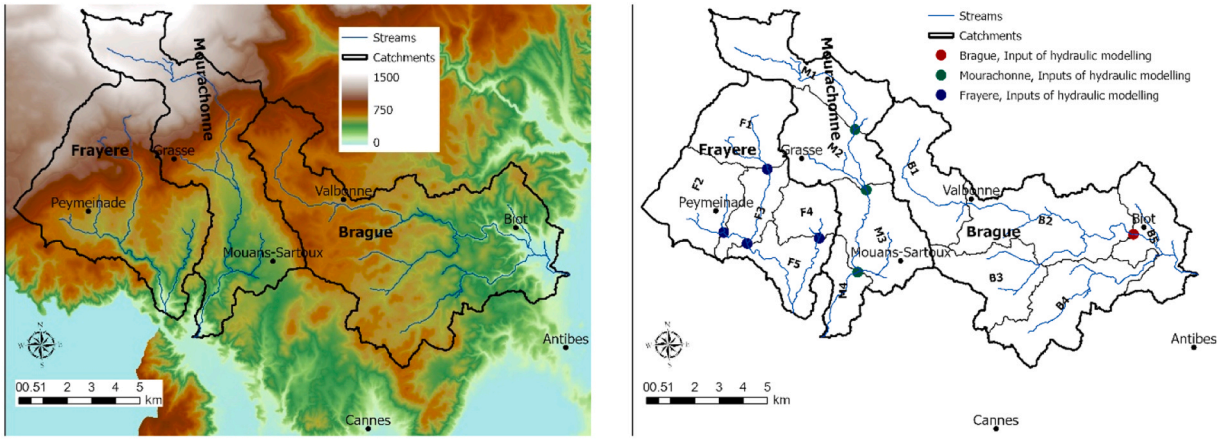

Fig. 1. a: Catchment limits and stream networks for the Frayère, Mourachonne and Brague. b: Study catchment subbasins and discharge input points for hydraulic model on the stream networks.

climate change.

The objective of this study is to analyse the impacts of urbanisation over 3 decades (1988/90–2020) on peak discharge and on flood exposure for rainfall events of different magnitudes in SE France. The study can be broken down into 3 sub-objectives: 1) to quantify historical changes in urbanisation, 2) to model the impacts of urbanisation on peak discharge, and 3) to model the impacts of urbanisation on flooded area and buildings affected. The study uses innovate methods to measure imperviousness based on building footprint layers and to quantify exposure based on the footprint area of buildings within the flooded zones.

2. Methods

The 3 study catchments are located in SE France. For each catchment, analysis was carried out in 3 steps corresponding to the sub-objectives defined above. Urbanisation rates were calculated from the building footprint layer, hydrologic modeling was performed using HEC-HMS, and hydraulic modeling was done using HEC-RAS.

2.1. Site description

The study catchments (Brague, Frayère and Mourachonne) are located near the cities of Antibes and Cannes in SE France (Fig. 1a). The Brague river (65.5 km^2) flows directly into the Mediterranean Sea whereas the Frayère and Mourachonne are tributaries of the Siagne. These two catchments (about 43 km^2) are therefore located further inland and have slightly steeper slopes and higher mean altitudes in the upper reaches (Table 1). For these catchments, steep slopes limit suburban expansion northwards, and potential flood plains are more restricted than for the Brague which has lower, flatter terrain near the outlet.

The catchments are located in a region of high potential employment. Tourism along the Mediterranean coast is the major source of revenue in the department, and the catchments include the high-tech business park of Sophia Antipolis and an internationally recognized perfume industry centered around the city of Grasse. Finally, the region is also known for its high number of secondary residential homes, so urban pressure is high.

The Brague catchment experienced a catastrophic flood in October 2015 when new rainfall intensity records were set with 2-hour maxima of about 150–175 mm; the estimated return period was greater than 100 years for the 1-hour and 2-hour rainfall intensities (Préfecture des Alpes-Maritimes, 2016).

2.2. Quantifying urbanization rates

Urbanization was quantified using 4 indicators: number of buildings, building footprint area, built area (area within a 100 m buffer around a building), and percentage imperviousness. The vector layer with building footprint polygons for each catchment was extracted from the BD-TOPO© national database. Working backwards in time, the 2020 building layer was successively overlain on ortho-rectified aerial photographs for 2014, 1999, 1990 (Brague) and 1988 (Frayère and Mourachonne). Spatial resolution for 1988/1990 and 1999 air photos was 50 cm; for 2014 and 2020 it was 20 cm. Buildings that were not present in a given year were deleted from the layer. Buildings that were present but had been destroyed in successive time intervals were hand-digitized.

Since the intervals between dates were not constant, all growth rates were normalized to decadal values. For example, the number of new buildings between 2014 and 2020 was divided by 6 and multiplied by 10. Similarly, the total interval for the Brague was 30 years, and for the Frayère and Mourachonne it was 32 years, so beginning-to-end comparisons were corrected to a 30-year equivalent time frame for the latter catchments. Absolute growth rates were also normalized for an equivalent catchment area of 50 km^2, an approximate intermediate surface area between Frayère/Mourachonne and Brague.

2.3. Hydrological modeling of river discharge

The Hydrologic Engineering Center Hydrological Modeling System (HEC-HMS) was used to model storm discharge for theoretical 12-hr rainfall events of 3 magnitudes: 80 mm, 140 mm, and 200 mm. Rainfall magnitude, duration and distribution were defined subjectively in order to produce events that were likely to generate moderate, large and extreme floods. The theoretical rainfall events used in this study were designed with a double-triangle shaped distribution (Benabdesselam and Hammar, 2009) so that 60 % of the rainfall was concentred in the center third of the hyetograph and 20 % before and after, respectively. The estimated 12-hour return period for 80 mm in the Brague is about 5 years, and for the 140 mm event it is about 75 years (Cabinet Merlin Ingénieurs Conseils, 2017). The return period for the 200 mm event is unknown but is probably in the order of about 300–400 years. Only peak discharge (Q_{peak}) at the outlet was retained for comparison between events, catchments and years as it can be most easily related to flood risk.

HEC-HMS simulates a wide range of hydrologic processes. Based on a 5 m DEM obtained from the National Institute for Geographic

Table 1
Catchment topographic characteristics.

Catchment	Area (km^2)	Mean slope (°)	Median slope (°)	Mean altitude (m)	Elevation range (m)
Brague	65.5	11.0	8.2	172.4	0–470
Frayère	42.2	14.3	12.1	374.7	21–1222
Mourachonne	43.6	12.7	9.8	448.7	14–1414

information (IGN), the model subdivides the catchment into subbasins according to topographic divides. The number of subbasins must be selected by the user, and 4 subbasins were retained for the Mourachonne and 5 for the Frayère and Brague, respectively (Fig. 1b). Model options for the simulations included the following: SCS-CN and Imperviousness for Loss, SCS Unit Hydrograph for Subbasin transform, Muskingum for Reach routing, Specified Hyetograph for Subbasin precipitation, a modeling timestep of 30 minutes, and baseflow.

The Curve Number (CN) for normal antecedent soil moisture conditions (CN II), time of concentration, and Muskingum X and K parameters were defined after a calibration and validation step on an event in the Brague catchment. The calibration event occurred 22 Nov., 2019 and had a Q_{peak} value of 135 $m^3 s^{-1}$, the validation event occurred 1 Dec., 2019, with a peak of 96 $m^3 s^{-1}$ (Fig. 2). Nash-Sutcliffe Efficiency (NSE) values for the calibration and validation simulations were 0.96 and 0.92, respectively, so the hydrologic model and parameter values selected below were deemed reliable. The calibrated values were applied to all catchments due to their similar characteristics.

A uniform CN value was used for all catchments and years, and the impact of urbanisation on discharge was quantified through changes in imperviousness. Although CN is spatially variable, differences here were considered minor since the only land cover types present in the catchments are urban/suburban and natural with a negligible area in grassland (golf course) located in the lower part of the Brague. In addition, the only land cover change between years is increased urbanisation, so finer mapping of CN outside urban areas would have had no impact on changes in discharge since the contribution of non-urban areas to runoff was constant over time. The CN value was set at 66 after calibration/validation simulations described above. An official report of the 2015 Brague flood indicates that a CN value of between 60 and 70 provided the closest simulated Q_{peak} values compared to field-estimated Q_{peak} values for the event (Lebouc and Payrastre, 2018), so it was deemed reasonable for the catchments

Temporal changes in Q_{peak} were simulated by changing the imperviousness value in the Loss function of HEC-HMS. It should be noted that this method uses total imperviousness for a subbasin and is less accurate than hydraulically connected imperviousness. This, however, is a limitation in the model that could not be modified and will be discussed further in the Discussion. In addition to buildings, imperviousness includes sidewalks, roads, parking lots and other impervious surfaces. These are spatially associated with the presence of buildings, so buffer zones (0–10 m, 10–20 m; 20–30 m and 30–100 m) were created around building polygons and reclassed with observed imperviousness according to values in Table 2. Imperviousness was calculated by overlaying random points on the 2020 ortho-rectified aerial photographs and counting the number of points that fell on pervious/impervious surfaces for each buffer zone and catchment. The number of random points per category ranged from 300 for the 0–30 m buffer zones to 600 for the 30–100 m buffer zone; 750 points were used for the zone beyond 100 m from a building. The random point method was done for 2020 and the spatial relationship was considered consistent over time. For each year, the calculated imperviousness layer was inputted into HMS in the format of a 5 m raster layer, and mean total imperviousness was extracted for each subbasin.

The time of concentration (T_c) for the SCS Unit Hydrograph was estimated for each subbasin after testing several formulae during the calibration/validation step. Lag time (T_L) was considered equal to 0.6* T_c as described in Chow et al. (1988); The calibration/validation step showed that the mean of the the Kirpich and Kerby methods provided the best estimate. The Muskingum X and K parameters were also defined during the initial calibration/validation step. at 0.2 and 0.6, respectively. Since the time intervals between years were not constant, the changes in Q_{peak} over time were standardized to an equivalent decadal interval: for example, for changes in 1990–1999, the change in Q_{peak} was divided by 9 and multiplied by 10. This enabled the direct comparison with urbanisation rates which were also standardized to the same interval.

Baseflow was attributed to subbasins closest to the outlet using the Recession method and an initial discharge of 2 $m^3 s^{-1}$ for the

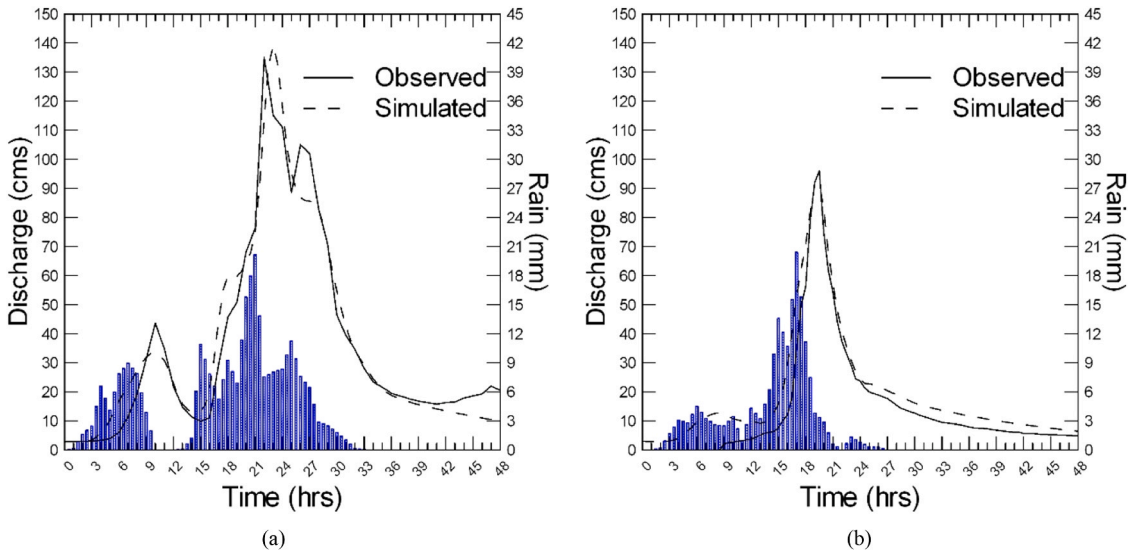

Fig. 2. a: Calibration simulation. b: Validation simulation.

Table 2
Imperviousness values attributed to buffer zones according to catchment and distance from buildings.

Buffer Zone (m)	Frayère-Mourachonne	Brague
Building	100.0	100.0
0–10	46.0	70.0
10–20	25.0	37.0
20–30	11.0	18.0
30–100	4.4	12.0
100 and more	0.9	3.5

Frayère and Mourachonne and of of 3 $m^3 s^{-1}$, for the Brague. A recession constant of 0.3, and a discharge threshold ranging from 20 to 30 $m^3 s^{-1}$ depending on the subbasin, were applied. In the field, initial discharge depends on a range of factors, so the values were selected to be typical for the catchments. The values were held constant for all rainfall events and years and were small compared to peak discharge (typically less than 3 %). The recession coefficient and discharge threshold values intervene after the peak discharge, so they have no impact on Q_{peak} results.

In all, 36 simulations were performed: 3 catchments (Brague, Frayère, Mourachonne), 4 years (1988/90, 1999, 2014, 2020), and 3 rainfall events (80 mm, 140 mm, 200 mm / 12 hours).

2.4. Hydraulic modeling of flooding risk

The Hydraulic Engineering Center River Analysis System (HEC-RAS) model was used for modeling the flooded area. No flood data were available to calibrate/validate the hydraulic modeling parameters, so reasonable values were selected from the scientific literature and HEC-RAS manual. Hydraulic modeling was carried out using a 1-m DEM obtained from the National Institute for Geographic information (IGN). A 30 m x 30 m mesh was used for most of the catchment, but this was reduced to 3 m x 3 m for channels, riverbanks, flood plains, and in regions defined as break lines (eg. roads, railways, levees…) in order to better simulate flow dynamics. Manning's roughness coefficient values (Manning's n) are shown in Table 3. Buildings were attributed an extremely high roughness to favor flow around buildings in open areas.

Input hydrographs for the hydraulic modeling were obtained from the outputs of the hydrologic model described above. For the Brague, a single input point was selected on the main channel upstream of the flood plain located in the lower part of the catchment (Fig. 2). For the Frayère, 4 input hydrographs were selected, and for the Mourachonne, 3 input hydrographs were selected (Fig. 2). As for the hydrological modeling, 36 simulations were performed, and 2 outputs were retained for comparison: total area flooded and building footprint area flooded. The flooded area of a building corresponded to the entire building footprint of the impacted building, even though only a portion of the building footprint may actually have intersected with the flooded area.

3. Results

The results are presented in order of the 3 sub-objectives defined above: urban expansion rates, change in peak discharge with urbanisation for rainfall events of different magnitude (hydrologic modeling), and changes in flooded area (hydraulic modeling) for each event.

3.1. Urbanisation trends

Urbanisation rates are presented firstly according to changes in the number of buildings and building footprint area and secondly according to changes in built area and total imperviousness.

3.1.1. New buildings and building area

In 1988/90, the Brague and Mourachonne have a similar number of buildings but the Brague has the greatest footprint area (Table 4). The Frayère has the most buildings but the smallest footprint area. Therefore, the Brague catchment has the largest initial mean building size and the Frayère has the smallest mean building size. In 2020, the Brague is approaching the Frayère in the number of buildings and continues to have the greatest footprint area, so it shows rapid growth over the duration of the study interval. Mean building size in the Brague shrinks slightly from 254.7 m^2 in 1990–246.8 m^2 in 2020. Corresponding values for the Frayère and Mourachonne show increases from 132.1 m^2 to 141.1 m^2 and 208.0 m^2 to 216.4 m^2, respectively. New buildings built between 1988/90 and 2020 had mean footprint areas of 234.7 m^2, 171.3 m^2 and 243.7 m^2 for the Brague, Frayère and Mourachonne, respectively.

Table 3
Manning's n values used for different land covers in the hydraulic simulations (Chow et al., 1988).

Building	Stream	Water body	Built area	Orchard vineyard	Grassland/ Shrubland	Cultivated	Forest
10.000	0.035	0.030	0.020	0.050	0.035	0.040	0.100

Table 4
Number of buildings and building footprint area for each year and catchment.

Catchment	Number of buildings				Building area (ha)			
	1988/90	1999	2014	2020	1988/90	1999	2014	2020
Brague	8703	10493	13568	14348	231.5	273.8	350.9	368.3
Frayère	11329	12874	14303	14667	151.7	179.9	202.4	209.9
Mourachonne	8598	10013	10985	11217	180.2	209.0	236.4	244.8

Standardized growth rates for the number of buildings (Fig. 3) show the fastest growth in the initial time interval with slowing over time for all catchments. Only the Brague maintains a constant rate into the second interval. Growth rates tend to be slightly greater for the Brague and lower for the Mourachonne. This corresponds to a 30-year equivalent increase of 5645, 3129, and 2455 new buildings in the Brague, Frayère and Mourachonne catchments, respectively, or increases of 64.9 %, 27.6 %, and 28.6 % in the number of buildings built between 1988/90 and 2020.

Changes in footprint area (Fig. 4) follow similar temporal and spatial patterns as building numbers, but building footprint area grows more slowly than the number of buildings in the Brague (59.1 % over 30 years) and more rapidly for the Frayère and Mourachonne (36.0 % and 33.6 %, respectively). As described above, this corresponds to a change in the mean building footprint where mean area decreases by 3.5 % for the Brague and increases by 6.4 % and 3.9 % for the Frayère and Mourachonne, respectively.

3.1.2. Changes in built area and imperviousness

Built area is calculated from building perimeter, so we would expect trends in building footprint area and built area to be more or less identical. However, adding new buildings within the buffer zones of existing buildings (ie. infilling between existing buildings in the built area) will increase the building footprint but not change the built area; hence, building footprint would increase much faster than built area. New buildings built outside the existing built area (ie. expansion) would cause built area to increase at the same relative rate as building footprint area. Therefore, the two numbers, building footprint area and built area, say something different about urban growth and to what extent growth is by infilling or expansion: for mainly infilling, building footprint area increases much faster than total built area, for expansion outside existing built area, built area growth trends are similar to building footprint growth rate.

The Brague has the greatest footprint area (Table 4) and built area in all years (Table 5). For the Frayère and Mourachonne, building footprint (Table 4) and built area (Table 5) follow the same patterns in 1988, where building area and built area are greater in Mourachonne than in Frayère, but the order is reversed starting in 1999; from then onwards, built area is greater in Frayère than Mourachonne. This indicates that more new buildings were built outside the perimeter of exiting built area in Frayère than in Mourachonne.

The trends described above are confirmed by the building footprint and built area growth rates shown in Fig. 4 and Fig. 5, respectively. In Fig. 4, the Mourachonne building footprint growth rates are equal to or greater than for the Frayère in all time intervals whereas the contrary is true in Fig. 5 where built area grows faster in the Frayère than in the Mourachonne in all time intervals. Over the 30-year equivalent time interval, built area grew more slowly than footprint area at rates of 34.1 %, 14.9 % and 15.8 % for the Brague, Frayère and Mourachonne, respectively (for comparison, rates shown above for building footprint area were 59.1 %, 27.6 %, and 28.6 %), so growth is shared roughly 50/50 between infilling and expansion into previously unbuilt areas.

Imperviousness is calculated from building footprint and buffer zones surrounding buildings where imperviousness decreases with distance from building perimeter as described in the Methods (Table 2). Changes in imperviousness therefore depend on initial imperviousness values when a new building is constructed: adding a new building next to an existing building where roads and parking lots, for example, are already present nearby increases imperviousness less than building on totally undeveloped land, sothe

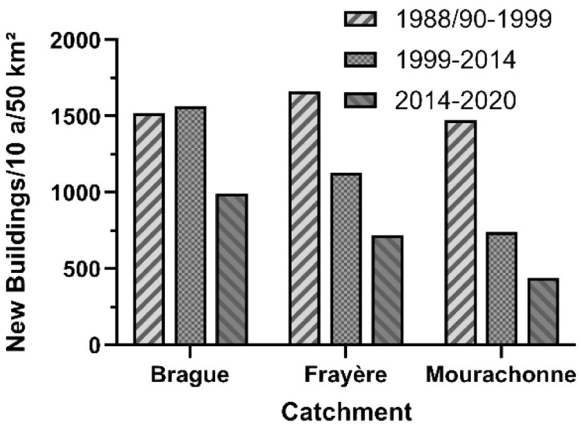

Fig. 3. Number of new buildings per decade per 50 km^2.

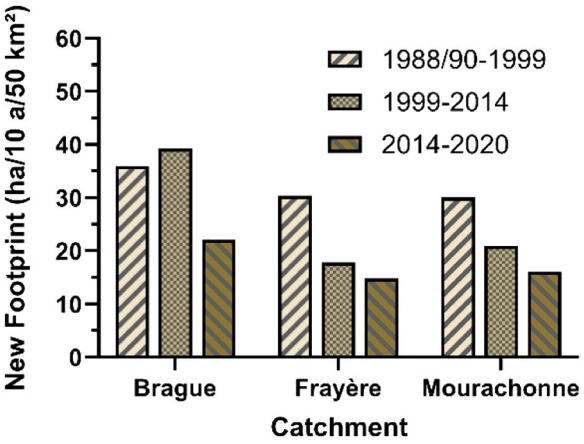

Fig. 4. Change in building footprint area per decade per 50 km^2.

Table 5
Built area and Imperviousness values for all years and catchments.

Catchment	Built area (km^2)				Imperviousness (%)			
	1988/90	1999	2014	2020	1988/90	1999	2014	2020
Bragues	2219.3	2516.0	2912.9	2975.3	20.1	22.4	25.7	26.4
Frayère	1856.2	2018.9	2131.0	2152.0	16.8	18.7	20.1	20.5
Mourachonne	1681.7	1832.7	1946.4	1965.3	14.6	16.2	17.6	17.9

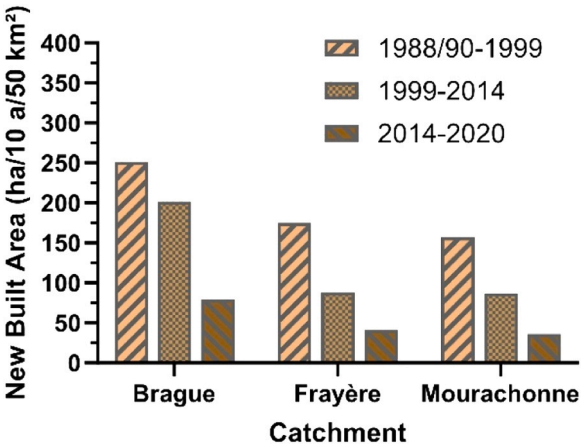

Fig. 5. Change in built area per decade per 50 km^2.

incremental increase in imperviousness is greater outside existing built area than within existing built area. Changes in imperviousness reflect a complex combination of changes in both new building footprint area and new built area. Temporal changes in imperviousness (Fig. 6) are consistent with changes in building area (Fig. 4) and built area (Fig. 5) where growth in imperviousness is greatest for the Bragues and similar for the Frayère and Mourachonne. Over the equivalent 30-year interval, imperviousness increases by 31.2 %, 20.6 % and 21.1 % for the 3 catchments, respectively.

3.1.3. Summary of urbanisation dynamics

Table 6 shows the ratios of percentage growth rates over the 30-year equivalent study interval. For example, in the Bragues, the growth rate in the number of buildings over 30 years was 64.9 % while the growth rate in the building footprint area was 59.1 %: the ratio is therefore 64.9 %/59.1 %, or 1.10 as shown in Table 6. Growth in the number of buildings in the Bragues is slightly greater than growth in building footprint area thereby indicating that buildings tend to get slightly smaller over time. The contrary is true for Frayère and Mourachonne where footprint area grows faster than the number of buildings (values <1.0).

The ratio of growth in building footprint to growth in built area (Table 6) is slowest for Bragues and greatest for Frayère, indicating

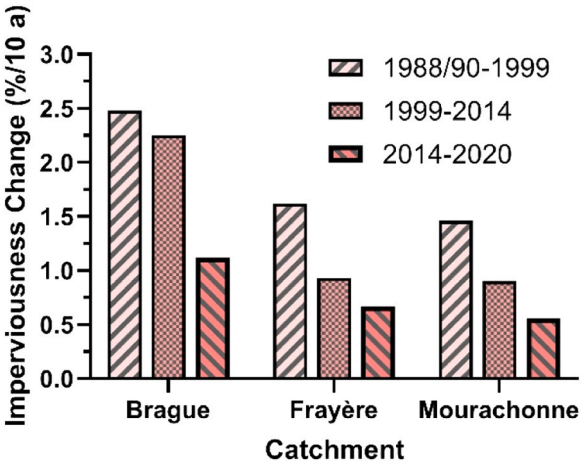

Fig. 6. Change in catchment imperviousness per decade.

Table 6
Ratios of 30-year equivalent relative growth rates.

Growth rate ratio	Bragues	Frayère	Mourachonne
Building numbers / building footprint	1.10	0.77	0.85
Building footprint / built area	1.73	2.41	2.13
Built area / Imperviousness	1.09	0.72	0.75

that of the three catchments, Bragues most strongly favours infilling over expansion compared to Frayère and Mourachonne, even though absolute built area growth in ha is greatest in the Bragues; hence a greater proportion of the Bragues's new building footprint is built within the perimeter of existing built area.

Built area growth rate is only slightly greater than imperviousness growth rate (Table 6) in the Bragues, and this is consistent with building in areas that are already partially impervious. For the Frayère and Mourachonne, imperviousness grows faster than built area since a greater proportion of the new buildings are built outside existing built area where the incremental increase in imperviousness with each new building is greater.

3.2. Impacts of urbanisation on peak discharge

Peak discharge values shown in Table 7 were not corrected for differences in area between catchments, but discharge ratios between catchments are very close to areal ratios: the Bragues's peak discharge is about 1.5 times the peak of the other catchments and its area is also about 1.5 times greater. Histograms for the simulations are provided in Appendix A. The Bragues therefore has the greatest peak discharge every year and for all rainfall magnitudes. For all catchments and events, peak discharge increases over time, which is consistent with the urbanisation trends described above.

Spatial evolutions in peak discharge (Fig. 7) follow urbanisation trends: the Bragues has the greatest increase in building area (Fig. 4), built area (Fig. 5) and imperviousness (Fig. 6) of the three catchments, and it shows the greatest increase in peak discharge. Temporal changes in peak discharge also closely resemble urbanisation patterns where peak discharge changes become smaller as urbanisation slows over time: for all catchments and rainfall events, the maximum change in peak discharge occurs in the 1988/90–1999 interval and the least change in the 2014–2020 interval. This pattern is true for all three rainfall events.

Table 7
Peak discharge values (m^3/s).

Catchment / Rainfall	1988/90	1999	2014	2020
Bragues (80 mm)	80.2	83.6	88.9	90.0
Bragues (140 mm)	230.3	234.6	241.6	243.1
Bragues (200 mm)	354.2	358.8	366.3	367.9
Frayère (80 mm)	55.8	57.6	59.2	59.6
Frayère (140 mm)	157.0	159.3	161.1	161.7
Frayère (200 mm)	241.7	244.0	245.9	246.4
Mourachonne (80 mm)	54.4	56.0	57.4	57.7
Mourachonne (140 mm)	157.2	159.0	160.5	160.9
Mourachonne (200 mm)	243.7	245.9	247.7	248.1

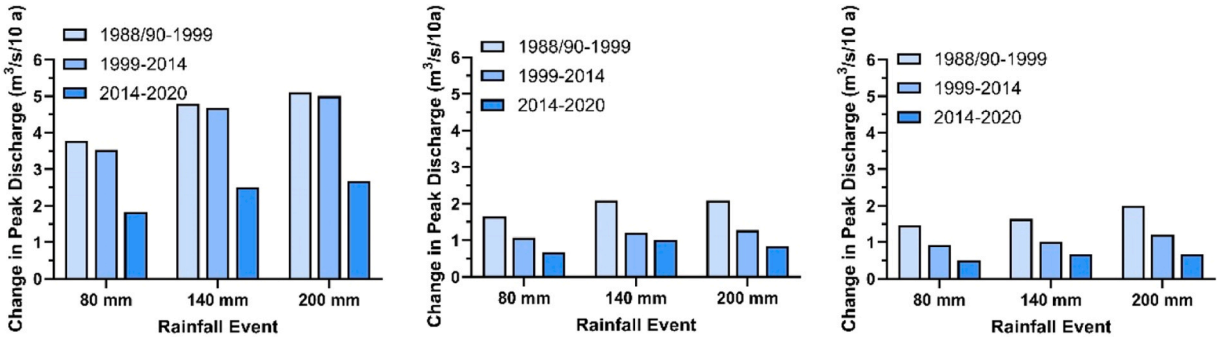

Fig. 7. Change in peak discharge (m^3/s per decade) according to temporal interval for Brague (left), Frayère (centre), and Mourachonne (right) and each rainfall event.

The impact of urbanisation on discharge is not independent of rainfall magnitude As rainfall magnitude increases, the increase in discharge within a time interval increases for all catchments: for the 80-mm rainfall event, the 30-year equivalent increases in discharge are 9.8 m^3/s, 3.8 m^3/s and 3.3 m^3/s for the Brague, Frayère and Mourachonne, respectively. Values for the 140 mm event are 12.8 m^3/s, 4.7 m^3/s and 3.7 m^3/s, and for 200 mm, they are 13.7 m^3/s, 4.7 m^3/s and 4.4 m^3/s, so the absolute increases are systematically smallest for the 80-mm event and greatest for the 200 mm event.

Although absolute discharge increases with rainfall magnitude, the relative increase in discharge is inversely proportional to the increase in rainfall magnitude. Fig. 8 shows the percentage increase in peak discharge for each time interval. The temporal patterns within the catchments remain the same as for absolute change in peak discharge (Fig. 7), but the patterns when comparing rainfall magnitude are reversed: absolute change in discharge increases with rainfall magnitude while relative increase in discharge decreases with rainfall magnitude. The percentage increase in peak discharge is always greatest for 80 mm and smallest for 200 mm. For 80 mm, the percentage increase in peak discharge is about 2.2–2.6 times greater than for 140 mm, and it is about 1.3–1.6 times greater for 140 mm than for 200 mm. In addition, these ratios generally decrease over time so differences in peak discharge for the same rainfall event get smaller over time. There are therefore two distinct trends: 1- changes in discharge over time get smaller as urbanisation rates slow, and 2- as rainfall magnitude increases, the relative impact of urbanisation on peak discharge decreases.

Overall, for the 80-mm rainfall event, the 30-year equivalent relative increases in discharge are 12.2 %, 6.8 % and 6.1 % for the Brague, Frayère and Mourachonne, respectively. Corresponding values for the 140 mm event are 5.6 %, 3.0 % and 2.4 %, and for 200 mm, they are 3.9 %, 1.9 % and 1.8 %. For comparison, changes in imperviousness at the catchment scale were 31.2 %, 21.6 % and 21.1 % for the Brague, Frayère and Mourachonne, respectively, as described above. Increases in peak discharge are therefore much smaller than corresponding increases in imperviousness.

3.3. Flood risk

The flooded area depends on urbanisation-driven changes in Q_{peak} described above, floodplain topographic characteristics specific to each catchment, and urbanisation rates within the flooded zone.

3.3.1. Spatial extent of flooded zone for different years and rainfall magnitudes

The spatial extent of the flooded zone (Table 8) changes with increases in discharge and local topographic conditions. Flooded area maps with building overlays are provided in Appendix B. As expected from the changes in peak discharge described above, all catchments show an increase in flooded area with increasing rainfall magnitude. The change is greatest for the Brague, which tends to have the smallest flooded area for the 80-mm event and the greatest area for the 140 and 200-mm events, where the flooded area is

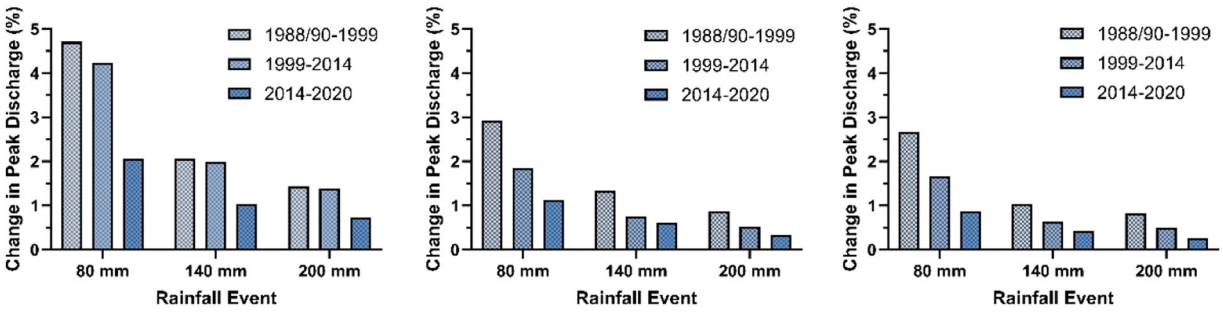

Fig. 8. Change in peak discharge (% per decade) according to temporal interval (% per decade) for Brague (left), Frayère (centre), and Mourachonne (right) and each rainfall event.

Table 8
Spatial extent (ha) of flooded zone for the different catchments, rainfall events and years.

Catchment / Rainfall	1988/90	1999	2014	2020
Brague (80 mm)	14.1	14.9	16.4	16.8
Brague (140 mm)	95.9	98.0	101.3	102.0
Brague (200 mm)	134.9	135.9	137.4	137.8
Frayère (80 mm)	22.3	22.7	22.9	23.0
Frayère (140 mm)	35.5	35.8	36.0	36.1
Frayère (200 mm)	43.8	43.9	44.1	44.1
Mourachonne (80 mm)	15.7	15.8	16.0	16.0
Mourachonne (140 mm)	40.1	40.3	40.4	40.4
Mourachonne (200 mm)	51.6	51.7	51.8	51.8

about 2.5–3 times greater than for the other catchments. Peak discharge values were only about 1.5 times greater for the Brague than for the other catchments, so the change in flooded area is clearly related to local topographic effects. The Brague has the lowest mean and median slope inclinations of the three catchments (Table 1) and, more particularly, an extensive flood plain of low slope where the flooded area expands rapidly for relatively small changes in flow depth.

Flooded area trends are consistent with the impacts of urbanisation on peak discharge; within each rainfall event, the temporal increase in flooded area (Fig. 9) follows the same patterns as urbanisation trends described above (Figs. 3–6). These changes, however, are much greater for the Brague than for the Frayère and Mourachonne. Over the equivalent 30-year study period, the Brague's flooded area increased by 2.7 ha, 8.7 ha and 5.3 ha for the 80-mm, 140-mm and 200-mm events respectively. Corresponding values for the Frayère and Brague are all less than 1.0 ha and generally less than 0.5 ha regardless of rainfall magnitude or time interval.

The relative increase in flooded area over time is shown in Fig. 10. Patterns within a rainfall event closely resemble urbanization trends and their impacts on Q_{peak}. Within each rainfall magnitude, the incremental increase in the extension of the flooded area over time diminishes with successive time intervals as urbanization rates slow. These changes vary with rainfall magnitude. The greatest relative impact is not for the 140-mm event (greatest absolute change) but for the 80-mm event, and values decrease with increasing rainfall magnitude. Since the absolute flooded area is relatively small for the 80-mm event, small changes have a greater impact on relative growth. And since the flooded area is already close to its maximum extent at 140-mm, and even more so at 200-mm, the gains in area over time due to urbanization do not translate into large relative growth rates.

3.3.2. Changes in footprint area in the flooded zone

Even if the flooded area had not grown over time, more buildings would have been exposed to flooding as new buildings were added to existing flood plains. The number of new buildings impacted by floods was quantified in this study, but since the overall trends were similar to built area, we retained only the latter in order to avoid redundancy.

As expected, flooded building footprint area increased with rainfall intensity within a year and over time. The Mourachonne had the greatest flooded building footprint, followed by the Brague and then the Frayère for the 80-mm event (Table 9). The Brague, however, rapidly surpassed the others as rainfall magnitude increased from 80 to 140 mm and again from 140 to 200 mm. This is consistent with the change in flooded area described above. The greatest absolute change in flooded building footprint area was for the 80 mm to 140 mm transition.

Flooded building footprint area (Fig. 11) increased most rapidly in the first interval (1988/90–1999), particularly in the Frayère and Mourachonne. For these catchments, growth rates drop abruptly after 1999. Growth rates in building footprint area in the flood zone are at their lowest after 2014. The Mourachonne even shows a loss of area with the destruction of some large hangars for the 200-mm event in 2014–2020.

The 30-year equivalent flooded zone footprint area growth rates are 76.3 %, 47.2 % and 33.4 % in the Brague for the 80-mm, 140-mm and 200-mm events, respectively. Corresponding values in the Frayère are 69.4 %, 62.3 % and 60.7 %, respectively. For the Mourachonne, they are 89.3 %, 43.0 % and 34.6 %, respectively, so growth in the Mourachonne is the greatest for the 80-mm event

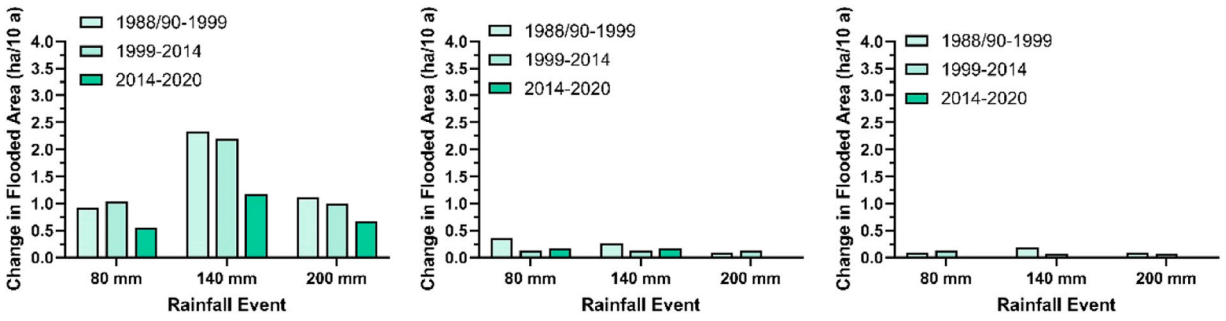

Fig. 9. Change in flooded area (ha/10 a) according to temporal interval and rainfall event for the Brague (left), Frayère (centre), and Mourachonne (right).

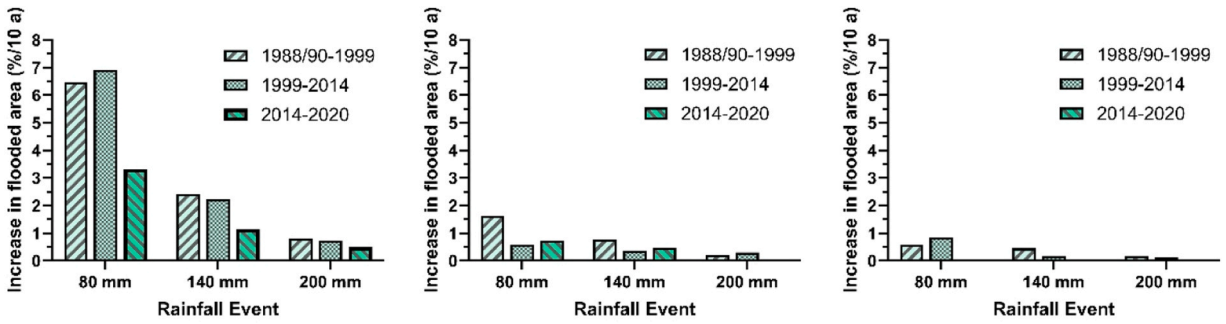

Fig. 10. Change in flooded area (%/10 a) according to temporal interval and rainfall event for the Bragueleft), Frayère (centre), and Mourachonne (right).

Table 9
Building footprint area in the flooded zone.

	Building footprint area (ha)		
Catchment / Year	**80 mm**	**140 mm**	**200 mm**
Bragueue 1990	0.93	7.94	10.70
Bragueue 1999	1.21	7.99	10.72
Bragueue 2014	1.64	11.59	14.27
Bragueue 2020	1.64	11.69	14.27
Frayère 1988	0.77	1.88	2.21
Frayère 1999	1.26	2.92	3.50
Frayère 2014	1.32	3.05	3.58
Frayère 2020	1.34	3.13	3.64
Mourachonne 1988	1.27	5.99	7.57
Mourachonne 1999	2.48	8.17	9.91
Mourachonne 2014	2.44	8.72	10.61
Mourachonne 2020	2.48	8.74	10.36

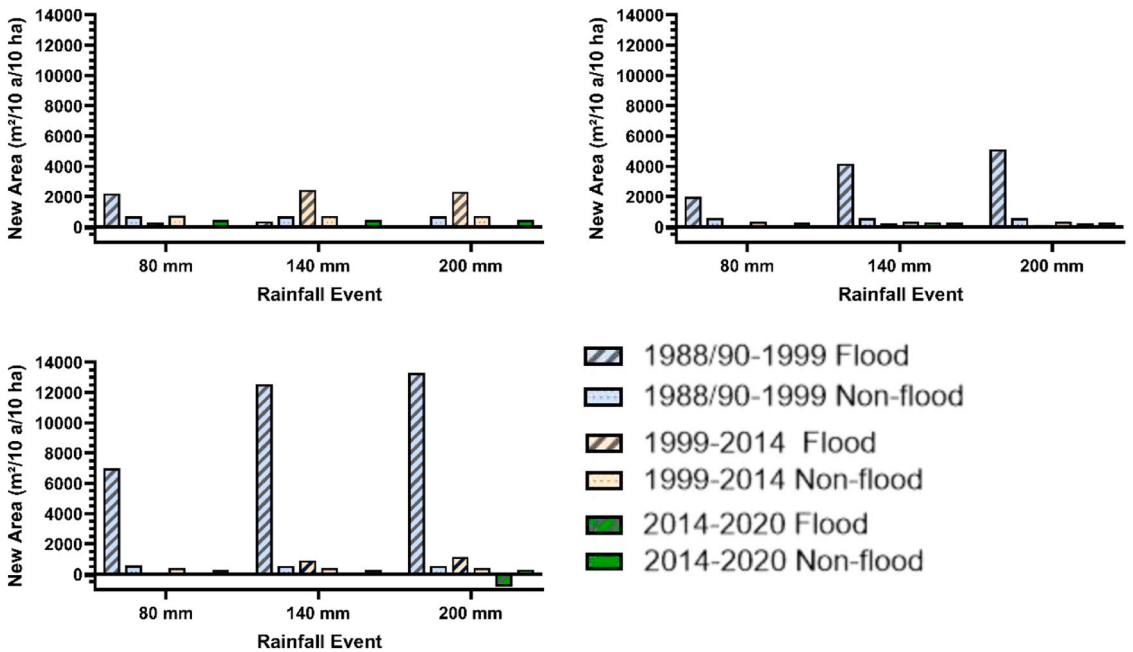

Fig. 11. Change in building footprint area within and outside the flood-zone for the Bragueleft), Frayère (top right) and Mourachonne (bottom left).

(buildings close to the channel). For all catchments, the relative growth in footprint area located in the flood zone diminishes with increasing rainfall magnitude. Initial building footprint area values are always lowest close to the channel (80-mm event), so the relative growth is greatest.

Flooded building footprint area increases with rainfall magnitude, but the relative increases with each increment in rainfall magnitude diminishes: between 1988/90 and 2020, as rainfall magnitude increases from 80 to 140 mm, the flooded building footprint area increases on average (mean of all years) by 633.4 %, 135.1 % and 277.7 %, for the Brague, Frayère and Mourachonne, respectively. As rainfall changes from 140 mm to 200 mm, the difference is only about 28.5 %, 17.8 % and 22.0 % for the same catchments. Hence, changes in exposure due to urbanisation in the flood zone over time were much greater as rainfall increased from 80 mm to 140 mm than for the 140 mm to 200 mm increment.

For comparison, the changes in flooded building footprint area outside the flooded zone are integrated in Fig. 11. For the non-flooded zone, the values are rough estimates since some slopes are too steep for construction, but the rate of building tends to be greater within the flooded zone than in the rest of the catchment. It is worth noting that the change in flooded building footprint area between 2014 and 2020 is negligible everywhere and for all rainfall events. This will be discussed further in the Discussion.

3.4. Summary of the interactions between urbanisation, hydrology and hydraulics

Urbanisation between 1988/90 and 2020 increased Q_{peak} by about 6 %-12 % for the 80 mm event depending on the catchment, and the increase diminished with greater rainfall magnitudes to attain about 2 %-4 % for the 200 mm event (Table 10). The change in Q_{peak} increased the total area flooded for all catchments and rainfall events. Similarly to Q_{peak}, the percentage increase in flooded area varied according to both catchment and rainfall event: the greatest increase for all events was for the Brague and the relative increase in area decreased with increasing rainfall magnitude. Changes in peak discharge depend on infiltration/runoff dynamics addressed below in the Discussion section whereas changes in flooded area depend on both peak discharge and local topography. For the Brague catchment, the percentage increase in flooded area is close to or surpasses the corresponding percentage increase in peak discharge (Table 10). The gap is greatest for the 80 mm event, where flat slopes close to the river channel allow rapid spreading of flood waters. For the 200 mm event, the percentage increase in flooded area over time is slightly less than the corresponding increase in peak discharge. For the Frayère and Mourachonne, the percentage increase in flooded area is always less than the corresponding increase in peak discharge. In these catchments, altitude increases quickly with distance from the river channels, so flooded area remains more contained than in the Brague.

The percentage differences between Q_{peak} and flooded area highlighted just above are relatively small, but the percentage differences between total flooded area and building footprint area flooded shown in Table 10 are substantial. On average, the percentage increase in the building footprint flooded is almost 43.4 times greater than the percentage increase in total flooded area; values range from 4.0 times greater for the Brague 80 mm event to 95.1 times greater for the Mourachonne 200 mm event.

Contrary to the preceding trends of Q_{peak} and flooded area, the ratio of the increase in number of buildings flooded to total flooded area increases with rainfall magnitude. As rainfall depth increases from 80 mm to 200 mm in the Brague, the ratio increases from 4.0 at 80 mm (ie. 76.3/19.1) to 15.5 (ie. 33.4/2.1) at 200 mm. Corresponding increases for the Frayère and Mourachonne are 23.6–94.5 and 49.9–95.1, respectively. Hence, urbanisation rates increased everywhere, but they were slowest nearest the channel and greatest further away. As flood magnitude increases, the number of buildings affected grows disproportionately large with respect to flooded area.

4. Discussion

Despite local catchment-scale differences, a number of trends identified in the study can be applied to most areas in the world undergoing rapid urbanisation.

4.1. Urbanisation and rainfall magnitude impacts on discharge

Both Q_{peak} and flooded area increased with urbanisation for all catchments. The increase in Q_{peak} with urbanisation was always less than the corresponding increase in imperviousness. This discrepancy between changes in imperviousness and peak discharge illustrates the distinction between total and effective imperviousness. Effective imperviousness is the share of the total imperviousness that is hydraulically connected to the channel (Alley and Veenhuis, 1983; Boyd et al., 1993; Ebrahimian et al., 2016), so our results indicate that a substantial portion of our imperviousness runs off onto pervious surfaces, as would be expected in suburban areas.

For the 80-mm event, the 30-year equivalent increase in Q_{peak} was about 3 times smaller than the corresponding increase in mean

Table 10
Percentage increase in hydrologic/hydraulic results over 30-year equivalent time interval for the three rainfall events (80 mm, 140 mm, 200 mm).

	Brague			Frayère			Mourachonne		
Variable	**80**	**140**	**200**	**80**	**140**	**200**	**80**	**140**	**200**
Q_{Peak}	12.2	5.6	3.9	6.8	3.0	1.9	6.1	2.4	1.8
Flood Area	19.1	6.4	2.1	2.9	1.6	0.6	1.8	0.7	0.4
Flooded footprint	76.3	47.2	33.4	69.4	62.3	60.7	89.3	43.0	34.6

catchment imperviousness, for the 140-mm and 200-mm events, the increase in Q_{peak} was about 7 and 10 times smaller, respectively, than the increase in imperviousness. The relative increase in Q_{peak} was greatest for the smallest rainfall event (80 mm) and diminished as rainfall magnitude increased. These results are consistent with theoretical expectations. Runoff coefficients increase with rainfall magnitude regardless of land cover type except for sealed surfaces which remain constant (Chow et al., 1988). As rainfall magnitude increases, spatial variations in runoff coefficients attributable to land cover type are progressively masked, so urbanisation has less impact on runoff for extreme events. This trend has been demonstrated in other cities around the globe (Braud et al., 2013; Yao et al., 2016; Zope et al., 2016) and confirms that the impact of urbanisation on discharge cannot be considered independently of rainfall magnitude. Theoretically, for immensely large rainfall magnitudes, Q_{peak} values would converge regardless of the land cover or percentage imperviousness.

4.2. Urbanisation and exposure to flooding

Urban expansion can increase exposure to flooding independently of changes in Q_{peak} and flooded area since there are more buildings exposed to flooding over time. Urbanisation was generally fastest in the initial time interval of the study (1988/90–1999) and slowed afterwards. This trend is true for all catchments and it surely reflects changes in regional economic and demographic drivers. In addition, more restrictive national risk management legislation was introduced in 1995 and implemented in the years afterwards, so most of the buildings affected by a flood were already built before the legislation was implemented, and the sharp drop in construction in the flood plain between 1988/90–1999 and 1999–2014 is probably due in part to the advent of the new flood risk planning laws. Flood risk planning legislation evolves spatially and over time (Borowska-Stefańska et al., 2021), and local urban planning legislation is continuously being updated, so it is impossible to work back through local planning rules for each of the municipalities located in the catchments. Despite protective legislation, building continued in all potential flood zones of the study, and the flooded building results show that the increase in flood risk depends more on greater exposure than on changes in Q_{peak}. This, too, is consistent with observations of others in the Mediterranean basin and in other regions of the world (Barredo et al., 2012; Flores et al., 2020; López-Martínez et al., 2017; Nguyen et al., 2021), and it is probably typical of most urbanised flood-prone zones globally. There is some flexibility in how urban planning rules are interpreted and implemented locally (Borowska-Stefańska et al., 2021; Winter and Karvonen, 2022), and elected officials are torn between economic interests in developing new activities on the one hand and protecting citizens on the other.

Urbanisation rates are slowest in the flooded area of the lowest magnitude event (80 mm) where new building growth is lower than for the rest of the catchment, and this suggests that building restrictions are historically greatest in the alluvial plain closest to the channel. Urban planning rules in France do not restrict all types of new buildings in a potential flood zone; urbanisation in areas of very high flooding risk is generally forbidden, but in areas of moderate flooding risk, some new construction is authorized. This includes buildings for activities that welcome the public during the day but not residential housing. Schools, libraries, sports facilities, concert venues, and some commercial/industrial activities, for example, can be authorized since these facilities can easily be pre-emptively closed or evacuated during the daytime in the case of extreme weather warnings. Residential buildings with no apartments on the ground floor may also be authorized in some cases. We assume that buildings built after 1999 in the 80-mm flood zone respect legislation in vigor at the time of construction and represent potential material flood damage but not necessarily greater human exposure as illustrated by the new industrial zone in the Mourachonne described above. New buildings flooded in the 140-mm and 200-mm flood zones, however, combine both greater infrastructure and human exposure.

Apart from the general slowing of urbanisation rates over time, the last time interval (2014–2020) corresponds to the 2015 catastrophic flood in the Brague. After 2014, building in the flooded zone was negligible, so independently of urban legislation, the study suggests that the catastrophic flood heightened awareness of the need to reduce exposure to floods. With regards to the 2015 flood, not only were the fatalities and extensive material damage traumatising, but the mayor of the main city (Biot) located in the catchment was convicted of involuntary homicide with a one-year suspended sentence for failing to take all the preventive measures necessary to ensure the security of the population as the event unfolded. Similarly, the mayor of La Faute sur Mer in western France was recently convicted of involuntary homicide after a dyke collapsed during the Xynthia storm of 2010 (53 fatalities in all, 29 in La Faute); he was deemed responsible for authorising the construction of new housing in a high risk coastal flood zone.

As the climate changes and the frequency and magnitude of extreme rainfall events increase (Ribes et al., 2019; Vautard et al., 2015), the greatest threat appears to be for buildings located in the flood zone defined in this study by the intermediate 140 mm rainfall event. Building restrictions will most likely always be greatest closest to the channel, so it is the zone just beyond this that will suffer most from an increase in extreme events. The 140 mm event is further and less restricted than for the 80-mm event, so the percentage increases in the buildings impacted attain their maximum values. The 200-mm event floods affect more area, but the relative growth in flooded area is more restricted as the limits of the flood plain are reached. The intermediate 80–140 mm transition therefore corresponds to the most dangerous transition in terms of the impact of urbanisation and climate change on flood risk.

4.3. Limitations and the potential for building footprint-based studies

The flooded building footprint area was probably overestimated in the hydraulic modeling calculations since flood depth was not explicitly taken into account and building design may have integrated measures to elevate new buildings that are not discernible from the footprint layer. For example, the large increase in the flooded building footprint area in the Mourachonne is related to a new industrial park built right next to the river channel. From the 2020 aerial photographs, we can see that several of these buildings are storage warehouses with loading platforms that appear to be at the height of the back end of a truck, so even though the parking lot would be flooded, it is unlikely the building itself would be submerged due to building design. The hydraulic model uses a 1-m DEM

where the flooded area corresponds to ground-level elevation. When a flooded depth of 20 cm is used as a criterion to evaluate the area of buildings impacted by a flood, the area retained in the Brague ranges from about 47 % of initial flooded building footprint area for the 80-mm event to 67 % for the 200 mm event. Corresponding values for the Frayère are 14–59 %, and for the Mourachonne they are 58–67 %. However, without extensive field investigation of every building, it is impossible to define local depth criteria more precisely, so values obtained here probably overestimate exposure, but the general trends remain unchanged.

Over a time-interval of 3 decades, substantial flood management work took place in all 3 catchments in the form of bank stabilisation, channel widening, and the introduction of retention dams on tributary channels, for example. The impacts of these measures on flooded area were not quantified here, but their beneficial effects on bankfull capacity are not without ambiguity, since they would probably also have impacted zoning rules with regards to flood risk. It is therefore probable that building in potential flood-affected zones over time was enabled partly by these improved flood control measures, but this was impossible to verify in the context of this study.

Finally, vector building layers have the potential to become the most accurate estimates of both exposure and vulnerability to floods since they can easily be crossed with several types of socio-economic data, including property values, average household income, employment rates, insurance rates… France has unique and extensive national-level GIS building footprint polygon layers and recent research has started to exploit the use of building footprint layers in flood studies (Hossain and Meng, 2020), including the Microsoft building footprint dataset released by Bing Maps for flood risk assessment for the Conterminous United States (Huang and Wang, 2020). Using building layers, the authors were able to identify weaknesses in traditional approaches (areas not previously covered, outdated data…) and a greater vulnerability of the poor to 100-yr floods. Similar databases are being developed for Europe (Florio et al., 2023; Milojevic-Dupont et al., 2023). The global availability of building footprint layers is therefore growing rapidly thanks to new building classification algorithms (Liu et al., 2022; Wei et al., 2022; Yu et al., 2023), so we can expect an exponential increase in the use of GIS building footprints in a range of hydrological and hydraulic approaches.

5. Conclusion

Urbanisation throughout the world increases flood risk as greater imperviousness increases both runoff and exposure as new buildings are added to a potential flood zone. Peak discharge increased with urbanisation between 1988/90 and 2020 at a rate that followed temporal trends in urbanisation rates. The increase in peak discharge increased the total flooded area and the area of buildings flooded. However, the relative increase in building area flooded was more than 40 times greater than the relative increase in total flooded area, and this demonstrates that the change in flooding risk was due more to greater exposure, as new buildings were added to the flooded zone, than to greater peak discharge values.

As rainfall magnitude increased from 80-mm to 200-mm, the total area and building footprint area flooded both increased. Closer to the channel, where the flooding risk is greatest, urban planning legislation provided some protection since the growth in flooded building area was lowest. As rainfall magnitude increased, less restricted areas further from the channel were exposed to flooding, and in these zones, the growth in flooding risk increased most. They were far enough from the channel to escape building restrictions, and the flatter terrain of the alluvial plain close to the main roads favoured rapid urbanisation. Hence, as rainfall magnitude increased, especially from 80 mm to 140 mm, the relative growth in buildings impacted was greatest. These intermediate zones in the alluvial plain present the greatest risk in a context of climate change where the magnitude and frequency of extreme events are expected to increase.

Data statement

Data will be made available on request.

Funding

This research was carried out within the framework of the FORESEE Project, supported by the Academy of Excellence 3 (Space, Environment, Risk and Resilience), and has been supported by the French government, through the UCA JEDI Investments in the Future project managed by the National Research Agency (ANR) with the reference number ANR-15-IDEX-01.

CRediT authorship contribution statement

Dennis M. Fox: Writing – review & editing, Writing – original draft, Supervision, Resources, Project administration, Methodology, Investigation, Funding acquisition, Formal analysis, Conceptualization. **Mostafa Banitalebi:** Visualization, Validation, Software, Methodology, Investigation, Formal analysis. **Anne Rainaud:** Writing – original draft, Conceptualization.

Declaration of Competing Interest

The authors declare that they have no known competing financial interests or personal relationships that could have appeared to influence the work reported in this paper.

Data availability

Data will be made available on request.

Appendix A. HEC-HMS Storm hydrographs

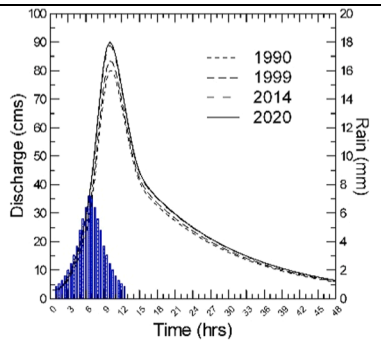

Figure A1.1: Bragué, 80 mm

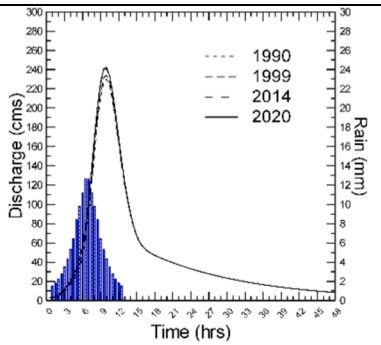

Figure A1.2: Bragué, 140 mm

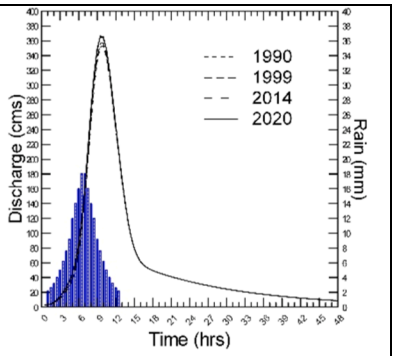

Figure A1.3: Bragué, 200 mm

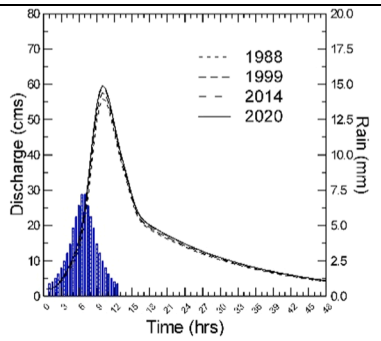

Figure A1.4: Frayère, 80 mm

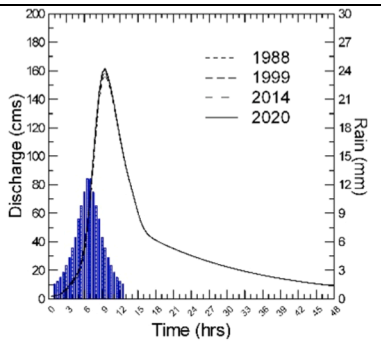

Figure A1.5: Frayère, 140 mm

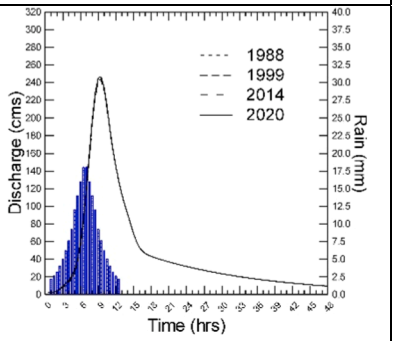

Figure A1.6: Frayère, 200 mm

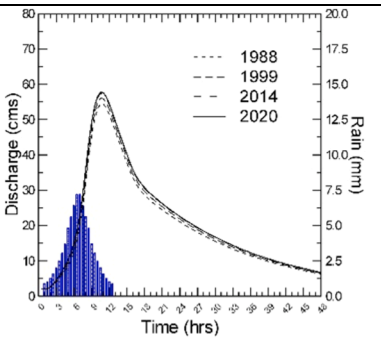

Figure A1.7: Mourachonne, 80 mm

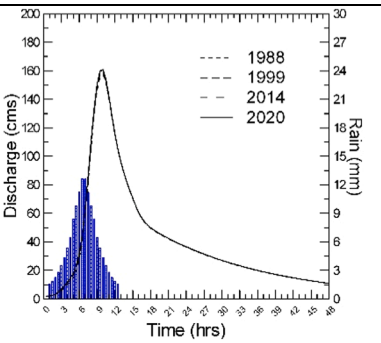

Figure A1.8: Mourachonne, 140 mm

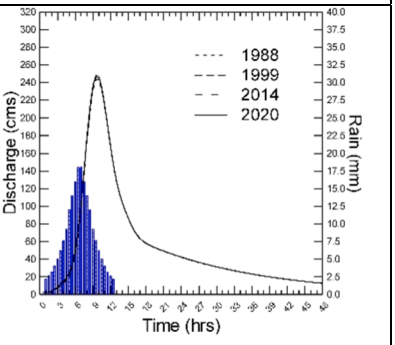

Figure A1.9: Mourachonne, 200 mm

Appendix B. HEC-RAS flooded areas with building overlays

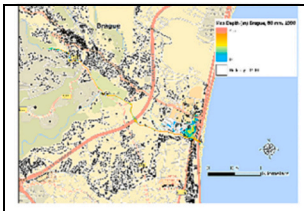	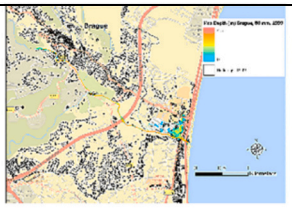	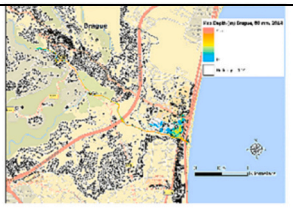	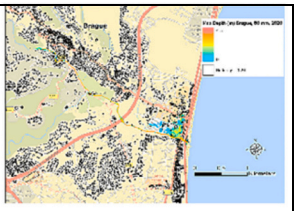
Figure B2.1: Bragues, 80 mm, 1990	Figure B2.2: Bragues, 80 mm, 1999	Figure B2.3: Bragues, 80 mm, 2014	Figure B2.4: Bragues, 80 mm, 2020
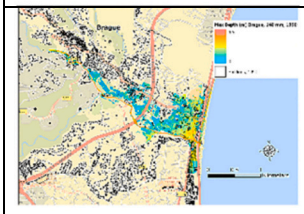	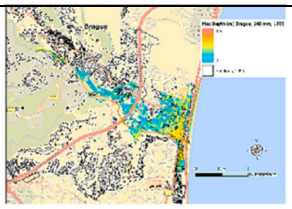	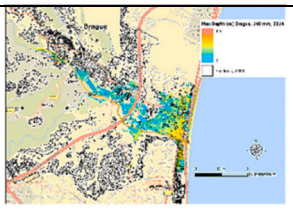	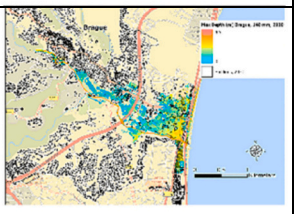
Figure B2.5: Bragues, 140 mm, 1990	Figure B2.6: Bragues, 140 mm, 1999	Figure B2.7: Bragues, 140 mm, 2014	Figure B2.8: Bragues, 140 mm, 2020
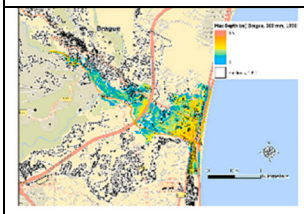	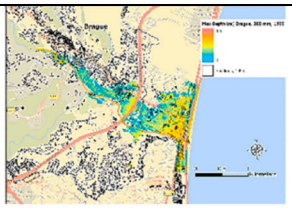	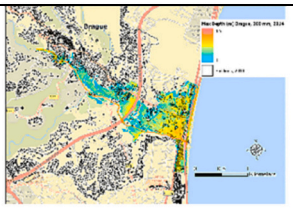	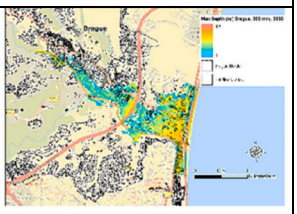
Figure B2.9: Bragues, 200 mm, 1990	Figure B2.10: Bragues, 200 mm, 1999	Figure B2.11: Bragues, 200 mm, 2014	Figure B2.12: Bragues, 200 mm, 2020
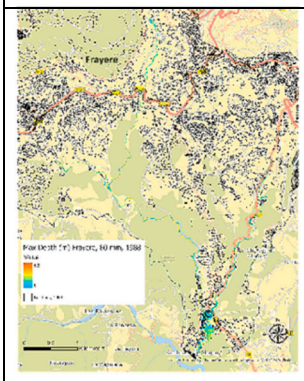	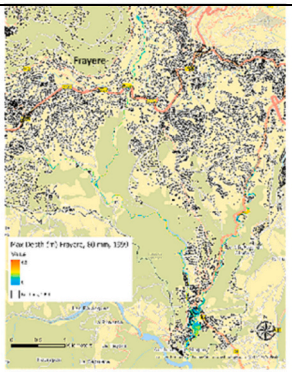	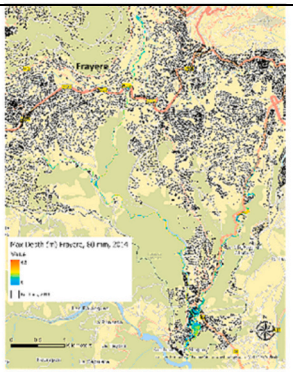	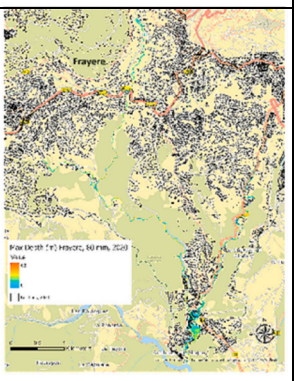
Figure B2.13: Frayère, 80 mm, 1990	Figure B2.14: Frayère, 80 mm, 1999	Figure B2.15: Frayère, 80 mm, 2014	Figure B2.16: Frayère, 80 mm, 2020

(continued on next page)

(*continued*)

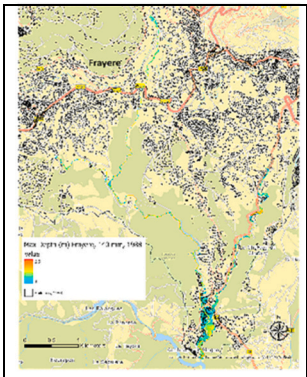	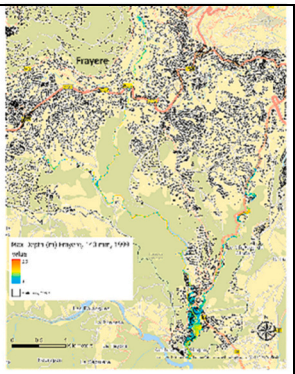	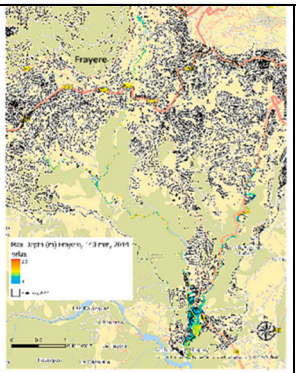	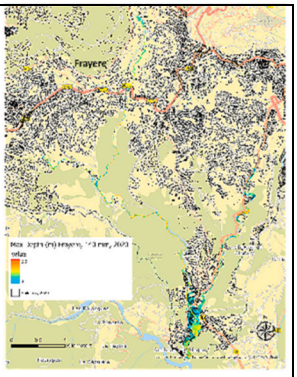
Figure B2.17: Frayère, 140 mm, 1990	Figure B2.18: Frayère, 140 mm, 1999	Figure B2.19: Frayère, 140 mm, 2014	Figure B2.20: Frayère, 140 mm, 2020
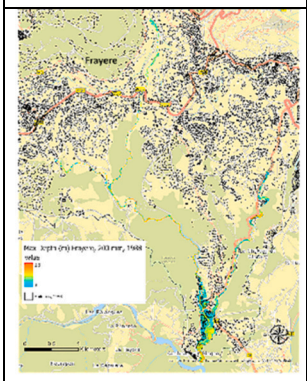	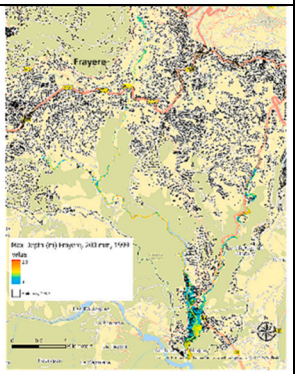	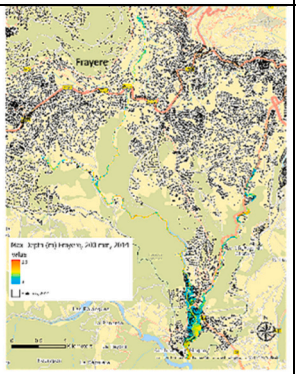	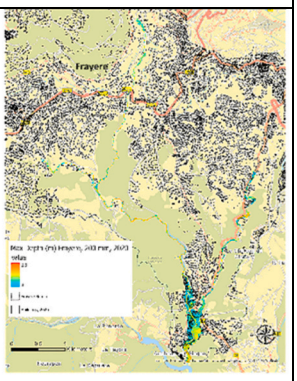
Figure B2.21: Frayère, 200 mm, 1990	Figure B2.22: Frayère, 200 mm, 1999	Figure B2.23: Frayère, 200 mm, 2014	Figure B2.24: Frayère, 200 mm, 2020
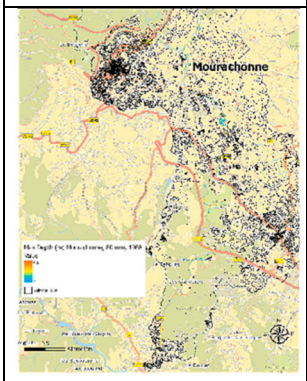	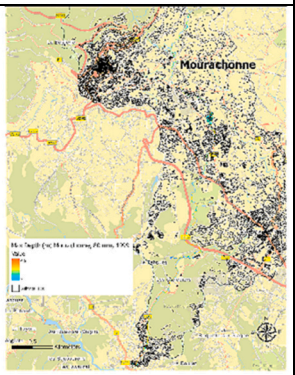	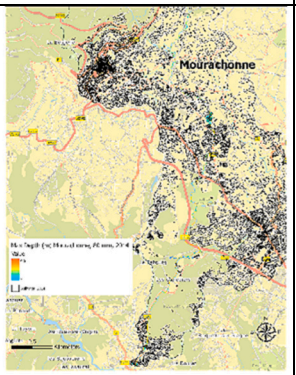	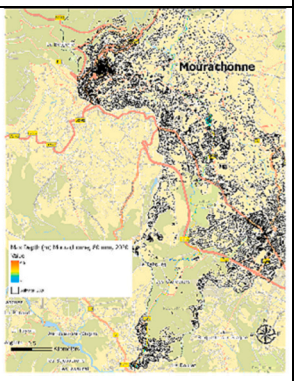
Figure B2.25: Mourachonne, 80 mm, 1990	Figure B2.26: Mourachonne, 80 mm, 1999	Figure B2.27: Mourachonne, 80 mm, 2014	Figure B2.28: Mourachonne, 80 mm, 2020

(*continued on next page*)

(*continued*)

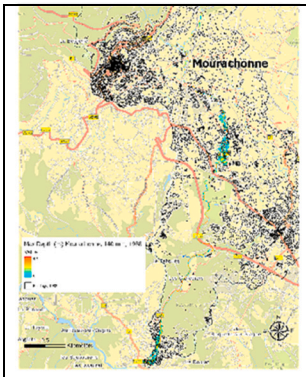	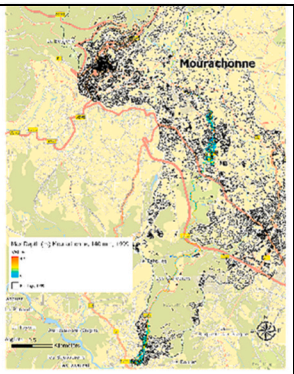	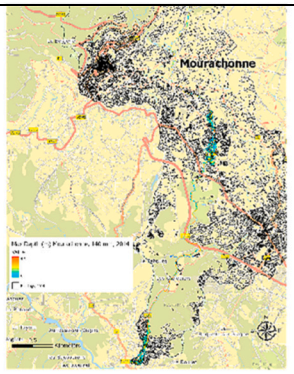	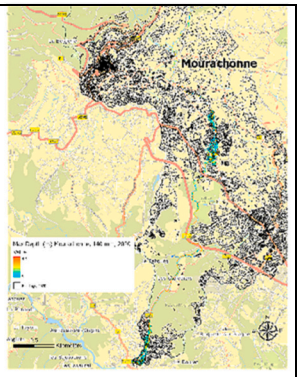
Figure B2.29: Mourachonne, 140 mm, 1990	Figure B2.30: Mourachonne, 140 mm, 1999	Figure B2.31: Mourachonne, 140 mm, 2014	Figure B2.32: Mourachonne, 140 mm, 2020
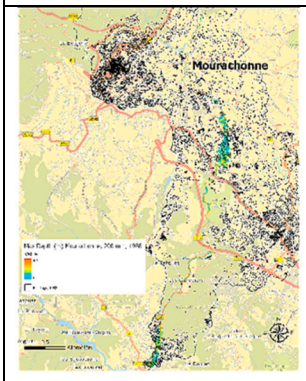	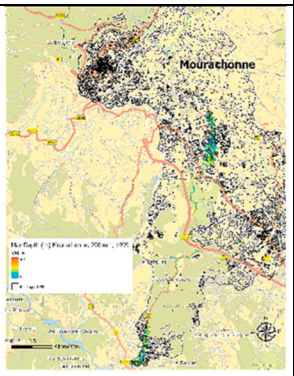	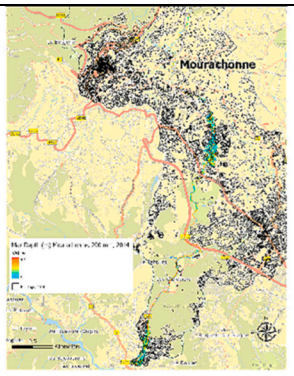	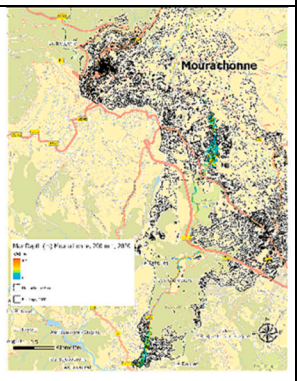
Figure B2.33: Mourachonne, 200 mm, 1990	Figure B2.34: Mourachonne, 200 mm, 1999	Figure B2.35: Mourachonne, 200 mm, 2014	Figure B2.36: Mourachonne, 200 mm, 2020

References

Ahiablame, L., Sinha, T., Paul, M., Ji, J.H., Rajib, A., 2017. Streamflow response to potential land use and climate changes in the James River watershed, Upper Midwest United States. J. Hydrol. Reg. Stud. 14, 150–166. https://doi.org/10.1016/j.ejrh.2017.11.004.

Alley, W.M., Veenhuis, J.E., 1983. Effective Impervious Area in Urban Runoff Modeling. J. Hydraul. Eng. 109, 313–319. https://doi.org/10.1061/(asce)0733-9429(1983)109:2(313).

Angel, S., Parent, J., Civco, D.L., Blei, A., Potere, D., 2011. The dimensions of global urban expansion: Estimates and projections for all countries, 2000-2050. Prog. Plann 75, 53–107. https://doi.org/10.1016/j.progress.2011.04.001.

Arnold, C.L., Gibbons, C.J., 1996. Impervious surface coverarge: the emergence of a key environmental indicator. J. Am. Plan. Assoc. 62, 243–258.

Barredo, J.I., Saurí, D., Llasat, M.C., 2012. Assessing trends in insured losses from floods in Spain 1971-2008. Nat. Hazards Earth Syst. Sci. https://doi.org/10.5194/nhess-12-1723-2012.

Benabdesselam, T., Hammar, Y., 2009. Estimation De La Réponse Hydrologique D'un Bassin Versant Urbanisé. Eur. J. Sci. Res. 29, 334–348.

Borowska-Stefańska, M., Kobojek, S., Kowalski, M., Lewicki, M., Tomalski, P., Wiśniewski, S., 2021. Changes in the spatial development of flood hazard areas in Poland between 1990 and 2018 in the light of legal conditions. Land Use Policy 102. https://doi.org/10.1016/j.landusepol.2020.105274.

Boyd, M.J., Bufill, M.C., Knee, R.M., 1993. Pervious and impervious runoff in urban catchments. Hydrol. Sci. J. 38, 463–478. https://doi.org/10.1080/02626669309492699.

Braud, I., Breil, P., Thollet, F., Lagouy, M., Branger, F., Jacqueminet, C., Kermadi, S., Michel, K., 2013. Evidence of the impact of urbanization on the hydrological regime of a medium-sized periurban catchment in France. J. Hydrol. (Amst. 485, 5–23. https://doi.org/10.1016/j.jhydrol.2012.04.049.

Cabinet Merlin Ingénieurs Conseils, 2017. Etude hydraulique et dossiers nécessaires à l'élaboration ou la révision des PPRI de 10 communes des Alpes Maritimes, Lot 1: Antibes - Biot - Vallauris. Alpes-Maritimes.

Chow, V. Te, Maidment, D.R., Mays, L.W., 1988. Applied Hydrology. McGraw-Hill.

De Luca, D.L., Ridolfi, E., Russo, F., Moccia, B., Napolitano, F., 2024. Climate change effects on rainfall extreme value distribution: the role of skewness. J. Hydrol. 634 https://doi.org/10.1016/j.jhydrol.2024.130958.
Ebrahimian, A., Wilson, B.N., Gulliver, J.S., 2016. Improved methods to estimate the effective impervious area in urban catchments using rainfall-runoff data. J. Hydrol. (Amst. 536, 109–118. https://doi.org/10.1016/j.jhydrol.2016.02.023.
Feyen, L., Dankers, R., Bódis, K., Salamon, P., Barredo, J.I., 2012. Fluvial flood risk in Europe in present and future climates. Clim. Change 112, 47–62. https://doi.org/10.1007/s10584-011-0339-7.
Flores, A.P., Giordano, L., Ruggerio, C.A., 2020. A basin-level analysis of flood risk in urban and periurban areas: A case study in the metropolitan region of Buenos Aires, Argentina. Heliyon 6. https://doi.org/10.1016/j.heliyon.2020.e04517.
Florio, P., Giovando, C., Goch, K., Pesaresi, M., Politis, P., Martinez, A., 2023. Towards a pan-eu building footprint map based on the hierarchical conflation of open datasets: the digital building stock model - DBSM. : Int. Arch. Photogramm., Remote Sens. Spat. Inf. Sci. - ISPRS Arch. Int. Soc. Photogramm. Remote Sens. 47–52. https://doi.org/10.5194/isprs-archives-XLVIII-4-W7-2023-47-2023.
Fox, D.M., Youssaf, Z., Adnès, C., Delestre, O., 2019. Relating imperviousness to building growth and developed area in order to model the impact of peri-urbanization on runoff in a Mediterranean catchment (1964-2014). J. Land Use Sci. 14 https://doi.org/10.1080/1747423X.2019.1681528.
Hossain, M.K., Meng, Q., 2020. A fine-scale spatial analytics of the assessment and mapping of buildings and population at different risk levels of urban flood. Land Use Policy 99. https://doi.org/10.1016/j.landusepol.2020.104829.
Huang, X., Wang, C., 2020. Estimates of exposure to the 100-year floods in the conterminous United States using national building footprints. Int. J. Disaster Risk Reduct. 50 https://doi.org/10.1016/j.ijdrr.2020.101731.
Jacobson, C.R., 2011. Identification and quantification of the hydrological impacts of imperviousness in urban catchments: A review. J. Environ. Manag. 92, 1438–1448. https://doi.org/10.1016/j.jenvman.2011.01.018.
Kundzewicz, Z.W., Pińskwar, I., Brakenridge, G.R., 2013. Large floods in Europe, 1985–2009. Hydrol. Sci. J. 58, 1–7. https://doi.org/10.1080/02626667.2012.745082.
Lebouc, L., Payrastre, O., 2018. Reconstitution et analyse des débits de pointe des crues du 3 octobre 2015 dans les Alpes Maritimes.
Liu, T., Yao, L., Qin, J., Lu, N., Jiang, H., Zhang, F., Zhou, C., 2022. Multi-scale attention integrated hierarchical networks for high-resolution building footprint extraction. Int. J. Appl. Earth Obs. Geoinf. 109 https://doi.org/10.1016/j.jag.2022.102768.
López-Martínez, F., Gil-Guirado, S., Pérez-Morales, A., 2017. Who can you trust? Implications of institutional vulnerability in flood exposure along the Spanish Mediterranean coast. Environ. Sci. Policy 76, 29–39. https://doi.org/10.1016/j.envsci.2017.06.004.
Milojevic-Dupont, N., Wagner, F., Nachtigall, F., Hu, J., Brüser, G.B., Zumwald, M., Biljecki, F., Heeren, N., Kaack, L.H., Pichler, P.P., Creutzig, F., 2023. EUBUCCO v0.1: European building stock characteristics in a common and open database for 200+ million individual buildings. Sci. Data 10. https://doi.org/10.1038/s41597-023-02040-2.
Myeong, S., Nowak, D.J., Hopkins, P.F., Brock, R.H., 2001. Urban Cover Mapping Using Digital, High-Spatial Resolution Aerial Imagery. Urban Ecosyst. 5, 243–256. https://doi.org/10.1023/A:1025687711588.
Nguyen, H.D., Fox, D., Dang, D.K., Pham, L.T., Viet Du, Q.V., Nguyen, T.H.T., Dang, T.N., Tran, V.T., Vu, P.L., Nguyen, Q.-H., Nguyen, T.G., Bui, Q.-T., Petrisor, A.-I., 2021. Predicting future urban flood risk using land change and hydraulic modeling in a river watershed in the central province of Vietnam. Remote Sens (Basel) 13. https://doi.org/10.3390/rs13020262.
Papalexiou, S., Montanari, A., 2019. Global and regional increase of precipitation extremes under global warming. WWR 55, 4901–4914. https://doi.org/10.1029/2018WR024067.
Préfecture des Alpes-Maritimes, 2016. Inondations des 3 et 4 octobre 2015 dans les Alpes-Maritimes: Retour d'Expérience. Préfecture des Alpes-Maritimes, Nice.
Prévost, A., Robert, S., 2016. Local spatial planning practices in four French Mediterranean coastal territories under pressure. Land Use Policy 56, 68–80. https://doi.org/10.1016/j.landusepol.2016.04.034.
Ribes, A., Thao, S., Vautard, R., Dubuisson, B., Somot, S., Colin, J., Planton, S., Soubeyroux, J.-M., 2019. Observed increase in extreme daily rainfall in the French Mediterranean. Clim. Dyn. 52, 1095–1114. https://doi.org/10.1007/s00382-018-4179-2.
Smiraglia, D., Cavalli, A., Giuliani, C., Assennato, F., 2023. The Increasing Coastal Urbanization in the Mediterranean Environment: The State of the Art in Italy. Land (Basel) 12. https://doi.org/10.3390/land12051017.
Sohn, W., Kim, J.H., Li, M.H., Brown, R.D., Jaber, F.H., 2020. How does increasing impervious surfaces affect urban flooding in response to climate variability? Ecol. Indic. 118, 106774 https://doi.org/10.1016/j.ecolind.2020.106774.
United Nations, Department of Economic and Social Affairs, Population Division, 2019. World Urbanization Prospects The 2018 Revision.
Vautard, R., Yiou, P., van Oldenborgh, G.-J., Lenderink, G., Thao, S., Ribes, A., Planton, S., Dubuisson, B., Soubeyroux, J.-M., 2015. Extreme Fall 2014 Precipitation in the Cévennes Mountains. Bull. Am. Meteor. Soc. 96, S56–S60. https://doi.org/10.1175/BAMS-D-15-00088.1.
Wagner, P.D., Bhallamudi, S.M., Narasimhan, B., Kantakumar, L.N., Sudheer, K.P., Kumar, S., Schneider, K., Fiener, P., 2016. Dynamic integration of land use changes in a hydrologic assessment of a rapidly developing Indian catchment. Sci. Total Environ. 539, 153–164. https://doi.org/10.1016/j.scitotenv.2015.08.148.
Wei, S., Zhang, T., Ji, S., Luo, M., Gong, J., 2022. BuildMapper: A Fully Learnable Framework for Vectorized Building Contour Extraction. https://doi.org/10.1016/j.isprsjprs.2023.01.015.
Winter, A.K., Karvonen, A., 2022. Climate governance at the fringes: Peri-urban flooding drivers and responses. Land Use Policy 117. https://doi.org/10.1016/j.landusepol.2022.106124.
Wu, C., Murray, A.T., 2003. Estimating impervious surface distribution by spectral mixture analysis. Remote Sens Environ. 84, 493–505.
Yang, J., Li, P., 2015. Impervious surface extraction in urban areas from high spatial resolution imagery using linear spectral unmixing. Remote Sens Appl. 1, 61–71. https://doi.org/10.1016/j.rsase.2015.06.005.
Yao, L., Wei, W., Chen, L., 2016. How does imperviousness impact the urban rainfall-runoff process under various storm cases? Ecol. Indic. 60, 893–905. https://doi.org/10.1016/j.ecolind.2015.08.041.
Yu, H., Hu, H., Xu, B., Shang, Q., Wang, Z., Zhu, Q., 2023. SuperpixelGraph: Semi-automatic generation of building footprint through semantic-sensitive superpixel and neural graph networks. Int. J. Appl. Earth Obs. Geoinf. 125, 103556 https://doi.org/10.1016/j.jag.2023.103556.
Zope, P.E., Eldho, T.I., Jothiprakash, V., 2016. Impacts of land use-land cover change and urbanization on flooding: A case study of Oshiwara River Basin in Mumbai, India. Catena (Amst.) 145, 142–154. https://doi.org/10.1016/j.catena.2016.06.009.